Subcell Modelling of Frequency Dependent Thin Layers in the FDTD Method

Kenan Tekbas, Fumie Costen, *Senior Member, IEEE*, Jean-Pierre Bérenger, *Fellow, IEEE*, Ryutaro Himeno, Hideo Yokota

***Index Terms*—Thin layer, subcell technique, Debye media, finite difference, FDTD, bioelectromagnetism.**

***Abstract*—A subcell modelling technique for frequency dependent thin layers in finite-difference time-domain (FDTD) method is introduced. The proposed method is based on the application of the integral form of the Maxwell-Ampere equation and the solution of a set of auxiliary equations to advance the field components. It has the ability to handle one or several frequency dependent thin layers embedded in a frequency dependent medium without solving high-order differential equations. To validate our proposed method, we compare the obtained results with analytical solutions and with numerical references in both time domain and frequency domain.**

I. Introduction

THE finite-difference time-domain (FDTD) method [1] relying on sampling the space and time is widely used for numerical simulations of electromagnetic wave propagation. The resolution of the sampling tends to be set under the Nyquist limit to retain the frequency components of interest in the system. However, when a very finely detailed geometry such as the Human-Body is in the FDTD space, the FDTD space has to be sampled in conformity with the thickness of the smallest details. This spatial sampling may be significantly shorter than the one needed for retaining the necessary frequency components. Furthermore, the overall number of FDTD cells and time steps may be excessively large with the very fine spatial resolution, rendering the computation impracticable.

In the past years, many works were conducted on accelerating the FDTD method by means of subcell techniques [1] that permit objects or structures thinner than the FDTD cell to be accounted for. The thin wire formalisms [2], [3] and thin slot formalisms [4], [5] have been the early subcell techniques. Later, several thin layer techniques [6]–[10] were published almost simultaneously to allow the FDTD method to deal with arbitrarily thin layers, without reducing the cell size in proportion. They can address dielectric and lossy materials where the real permittivity and the conductivity are not frequency dependent, and they assume that the layer is thin with respect to the wavelength and the skin depth. More recently, methods relying on the same assumption have been reported [11], [12] to account for layers where the permittivity and the permeability are frequency dependent complex numbers. And to address the opposite situation of [6]–[12], that is the case where the skin depth in the layer is shorter than its thickness, there exist other thin layer methods based on the surface impedance boundary condition concept, as the recent work [13].

In this paper, we present a method which permits one or several frequency dependent thin layers to be embedded in a frequency dependent background. This is a situation currently encountered in bioelectromagnetism where thin layers are placed between thick media. Such problems cannot be addressed with [11], [12] that deal with only one dispersive layer surrounded with a vacuum. The proposed method relies on the application of the integral form of the Maxwell-Ampere equation and the solution of a set of auxiliary equations.

Section II describes the principle of the method. Section III derives the FDTD equations for the advance of the electric and magnetic fields in the cells traversed by the layers. Section IV is devoted to numerical experiments. Comparisons with analytical solutions and with numerical references, in both time domain and frequency domain and in one dimension(1D) and three dimensions(3D), clearly demonstrate the accuracy of the method. Finally, Section V proposes a simplified version of the thin layer method that can yield an acceptable approximation of the rigorous solution in some Human-Body applications.

II. The Principle of the Thin Layer Technique for Debye Media

A. The Debye Media in the FDTD Method

In bioelectromagnetism, the electrical properties of the human tissues are in general described by the Debye model where the relative permittivity is complex and frequency dependent. The one-pole Debye model reads

$$\epsilon_r(\omega) = \epsilon_\infty + \frac{\epsilon_\mathrm{S} - \epsilon_\infty}{1 + \jmath\omega\tau} + \frac{\sigma}{\jmath\omega\epsilon_0} \tag{1}$$

where ϵ_0 is the vacuum permittivity, ϵ_∞ is the optical relative permittivity, ϵ_S is the static relative permittivity, τ is the relaxation time, σ is the conductivity and ω is the angular frequency of $2\pi f$. The relationship that connects the electric field component E_u and the electric flux density D_u is then

$$D_u(\omega) = \epsilon_0 \left[\epsilon_\infty + \frac{\epsilon_\mathrm{S} - \epsilon_\infty}{1 + \jmath\omega\tau} + \frac{\sigma}{\jmath\omega\epsilon_0}\right] E_u(\omega), (u = x, y, z). \tag{2}$$

Equation (2) can be written as

$$(\jmath\omega)^2\tau D_u + (\jmath\omega) D_u = (\jmath\omega)^2\epsilon_0\epsilon_\infty\tau E_u + \jmath\omega(\epsilon_0\epsilon_\mathrm{S} + \sigma\tau)E_u + \sigma E_u. \tag{3}$$

K. Tekbas, F. Costen, and J.P. Bérenger are with the School of Electrical and Electronic Engineering, The University of Manchester, U.K. (email: fumie.costen@manchester.ac.uk)

R. Himeno is Advanced Center for Computing and Communication, RIKEN, Saitama, Japan

H. Yokota and F. Costen are with the Image Processing Research Team, Center for Advanced Photonics, RIKEN, Saitama, Japan.

The time domain counterpart of (3) can be obtained by replacing $\jmath\omega$ with the derivative on time $\dfrac{\partial}{\partial t}$. This yields

$$\tau\frac{\partial^2 D_u}{\partial t^2}+\frac{\partial D_u}{\partial t}= \epsilon_0\epsilon_\infty\tau\frac{\partial^2 E_u}{\partial t^2}+(\epsilon_0\epsilon_{\rm S}+\sigma\tau)\frac{\partial E_u}{\partial t}+\sigma E_u. \quad (4)$$

Equation (4) is used as an auxiliary equation in the FDTD method in Debye media. More precisely, at each time step the D_u component is advanced by means of the discretised Maxwell-Ampere equation, and then E_u is obtained from D_u by the discretised form of (4) in [14].

B. The Previous Thin Layer Methods

The methods [6]–[10], presented independently, are all based on the same principle. They consist of computing the electric components parallel to the layer by discretising the integral form of the Maxwell-Ampere equation

$$\iint_S \frac{\partial \boldsymbol{D}}{\partial t}ds=\oint_C \boldsymbol{H}dl \quad (5)$$

in place of its differential form usually employed in the FDTD method. In (5), C is the contour that surrounds a surface S which is that of one cell in the FDTD discretisation. Use of the integral form permits cells filled with several media to be accounted for, which is not possible with the differential form. The methods [6]–[10] are fundamentally similar in their assumptions. Only [7] significantly differs from the others because it assumes that the electric component normal to the layer is present in the layer, which results in a special FDTD advance of this component in addition to special advances of the other two components. The rationale to do this is not provided in [7], it is just reported in [9] that in special cases where the parallel components are negligible, the results are slightly improved by this additional treatment. The thin layer method presented in the following also relies on the disretisation of (5) for the advance of the electric components parallel to the layer. There is no special treatment of the component normal to the layer. The method can then be viewed as an extension of methods [8] and [10] which are identical, even if there are more theoretical investigations of the accuracy in [10].

C. The Equations to be solved in the FDTD cells crossed by the thin layer

Let us consider a layer of thickness d perpendicular to direction x and placed between two frequency dependent media as represented in Fig. 1. The components E_y and E_z are parallel to the layer and located inside it. This is the same arrangement as in [6]–[10]. Fig. 2 shows a x-y plane with a layer in the middle of a FDTD cell, with E_z node inside the layer and the $\boldsymbol{H}$ components surrounding it. The tangential D_z is not continuous at the interfaces between the three media, so that three different D_z must be considered in the cell. Let us denote them as D_{z_1}, D_{z_2} and D_{z_3}. Assuming that $\boldsymbol{E}$ and $\boldsymbol{D}$ are computed at time n and $\boldsymbol{H}$ at time $n+\frac{1}{2}$

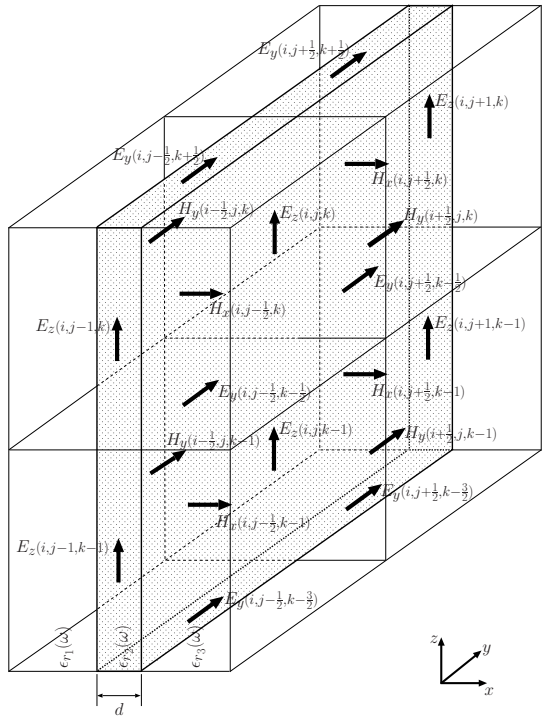

Fig. 1. Thin layer and the field components in the three-dimensional FDTD grid.

in the grid, applying the Maxwell-Ampere equation (5) to the surface $\Delta x\Delta y$ in Fig. 2 yields

$$\left[\frac{\partial \Psi_{z(i,j,k)}}{\partial t}\right]^{n+\frac{1}{2}}\Delta x\Delta y=C^{n+\frac{1}{2}} \quad (6)$$

where

$$C^{n+\frac{1}{2}}=H_x^{n+\frac{1}{2}}(i,j-\tfrac{1}{2},k)\Delta x-H_x^{n+\frac{1}{2}}(i,j+\tfrac{1}{2},k)\Delta x + H_y^{n+\frac{1}{2}}(i+\tfrac{1}{2},j,k)\Delta y-H_y^{n+\frac{1}{2}}(i-\tfrac{1}{2},j,k)\Delta y$$

and $\Psi_{z(i,j,k)}$ is an auxiliary quantity homogeneous to $\boldsymbol{D}$, defined as the sum of the D_z components weighted with the partial surfaces in the cell

$$\Psi_{z(i,j,k)}=s_1D_{z_1(i,j,k)}+s_2D_{z_2(i,j,k)}+s_3D_{z_3(i,j,k)} \quad (7)$$

with

$$s_2=\frac{d}{\Delta x},\qquad s_1=s_3=\frac{1}{2}-\frac{d}{2\Delta x}.$$

Assuming that Ψ_z is known at the same time n as E_z and D_z, it can be advanced to time $n+1$ by discretising the derivative in (6). This gives

$$\Psi_z^{n+1}=\Psi_z^n+\frac{C^{n+\frac{1}{2}}}{\Delta x\Delta y}\Delta t. \quad (8)$$

The final objective is to find the E_z component at time $n+1$ in the FDTD cell, because it is needed for the advance of the $\boldsymbol{H}$ field at the next half-step of the FDTD time stepping. The tangential E_z component is continuous at the interfaces between the media. Therefore, it can be assumed as uniform in the cell in Fig. 2, as in any other cell of the FDTD space. In theory, finding E_z at time $n+1$ can be done by means of two methods. They are described in the following:

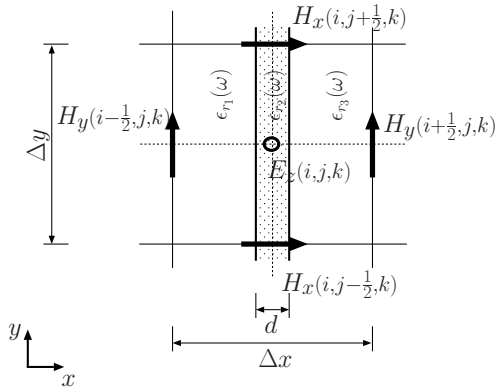

Fig. 2. A cross-section of a $\Delta x \times \Delta y \times \Delta z$ FDTD cell with a frequency dependent layer of thickness d placed between two frequency dependent media.

1) Advance of the E field by solving a $(M+1)$-order differential equation for M different Debye materials in the cell : The method consists of writing (7) in frequency domain, which reads

$$\Psi_z(\omega) = s_1 D_{z_1}(\omega) + s_2 D_{z_2}(\omega) + s_3 D_{z_3}(\omega) \tag{9}$$

where the location (i,j,k) has been omitted. Since E_z is the same in the three media and also $D_z(\omega) = \epsilon(\omega) E_z(\omega)$ holds in each medium, (9) can be written as

$$\Psi_z(\omega) = \epsilon_0 [s_1 \epsilon_{r_1}(\omega) + s_2 \epsilon_{r_2}(\omega) + s_3 \epsilon_{r_3}(\omega)] E_z(\omega). \tag{10}$$

This expression is general *i.e.*, valid with any media. In the special case of Debye media (1), it can be explicitly written as

$$\Psi_z(\omega) = \epsilon_0 \left[\sum_{m=1}^{3} s_m \epsilon_{\infty_m} + \sum_{m=1}^{3} s_m \frac{\epsilon_{\mathrm{S}_m} - \epsilon_{\infty_m}}{1 + \jmath\omega\tau_m} + \sum_{m=1}^{3} s_m \frac{\sigma_m}{\jmath\omega\epsilon_0} \right] E_z(\omega) \tag{11}$$

where ϵ_{∞_m},ϵ_{S_m}, τ_m and σ_m are the Debye parameters of medium m. Equation (11) is in the same form as (2) that holds at every E_z node in the Debye medium, with just $\Psi_z(\omega)$ in place of $D_z(\omega)$ and the bracket in (11) in place of permittivity $\epsilon_r(\omega)$ in (2). From this, E_z^{n+1} is the function of the known Ψ_z^{n+1}. Let us first consider the case where only medium 2 is a Debye medium, the other two being pure dielectric or lossy media. Then (11) reduces to

$$\Psi_z(\omega) = \epsilon_0 \left[\langle \epsilon_\infty \rangle + s_2 \frac{\epsilon_{\mathrm{S}_2} - \epsilon_{\infty_2}}{1 + \jmath\omega\tau_2} + \frac{\langle \sigma \rangle}{\jmath\omega\epsilon_0} \right] E_z(\omega) \tag{12a}$$

where

$$\langle \epsilon_\infty \rangle = s_1 \epsilon_{r_1} + s_2 \epsilon_{\infty_2} + s_3 \epsilon_{r_3}, \tag{12b}$$

$$\langle \sigma \rangle = s_1 \sigma_1 + s_2 \sigma_2 + s_3 \sigma_3. \tag{12c}$$

Equation (12a) is the same as (2), with just other coefficients. Its time domain counterpart can be written as

$$\tau_2 \frac{\partial^2 \Psi_z}{\partial t^2} + \frac{\partial \Psi_z}{\partial t} = \epsilon_0 \langle \epsilon_\infty \rangle \tau_2 \frac{\partial^2 E_z}{\partial t^2} + (\epsilon_0 \langle \epsilon_{\mathrm{S}} \rangle + \langle \sigma \rangle \tau_2) \frac{\partial E_z}{\partial t} + \langle \sigma \rangle E_z \tag{13a}$$

with

$$\langle \epsilon_{\mathrm{S}} \rangle = s_1 \epsilon_{r_1} + s_2 \epsilon_{\mathrm{S}_2} + s_3 \epsilon_{r_3} \tag{13b}$$

which is identical to (4) rigorously, with just the permittivities and the conductivity replaced with the weighted averaged values of (12b), (12c) and (13b), and with the relaxation time τ_2 of the thin layer. Thus, when a thin layer is placed between two dielectric or lossy media, and especially in a vacuum, E_z^{n+1} can be obtained using the same equation as at any regular node of the grid, with (12b), (12c), (13b) and $\tau = \tau_2$.

In the case where several Debye media are present, replacing $\jmath\omega$ with $\dfrac{\partial}{\partial t}$ in (11) yields a differential equation connecting Ψ_z and E_z. Its order is $M+1$ when M Debye media are present. For example (11) becomes a 4-order differential equation when three Debye media are present. It could be discretised to provide us with E_z^{n+1} in function of Ψ_z^{n+1}. However, the high-order discretisation would be complicated. This is why we used this method only with $M = 1$ which yields (13). For $M > 1$ we used the other solution presented in the next section.

2) Advance of the E field by solving a set of 2-order differential equations: This method to find E_z^{n+1} from Ψ_z^{n+1} requires expressing D_{z_m} $(1 \le m \le M)$ in function of the common E_z by using M relationships of $D_{z_m} = \epsilon_m(\omega) E_z(\omega)$ which hold in the media

$$D_{z_m}(\omega) = \epsilon_0 \left[\epsilon_{\infty_m} + \frac{\epsilon_{\mathrm{S}_m} - \epsilon_{\infty_m}}{1 + \jmath\omega\tau_m} + \frac{\sigma_m}{\jmath\omega\epsilon_0} \right] E_z(\omega) \tag{14}$$

which are identical to (2) used at the regular nodes of the FDTD space to find E_z^{n+1} from D_z^{n+1}. Their time domain counterparts are the same as well, which read

$$\tau_m \frac{\partial^2 D_{z_m}}{\partial t^2} + \frac{\partial D_{z_m}}{\partial t} = \epsilon_0 \epsilon_{\infty_m} \tau_m \frac{\partial^2 E_z}{\partial t^2} + (\epsilon_0 \epsilon_{\mathrm{S}_m} + \sigma_m \tau_m) \frac{\partial E_z}{\partial t} + \sigma_m E_z, (1 \le m \le M). \tag{15}$$

Discretisation of (15) provides us with M equations connecting $D_{z_m}^{n+1}$ to E_z^{n+1}. These equations with (7) and (8) form simultaneous equations for the unknowns E_z^{n+1} and $D_{z_m}^{n+1}$. Therefore, the advance to time step $n+1$ can be completed in the cell. Notice that in the special case where a thin layer is placed in a vacuum, $M-1$ out of M equations in (15) reduce to $D_{z_m}^{n+1} = \epsilon_0 E_z^{n+1}$ and thus only one 2-order differential equation is used, as in the previous method with (13a).

In summary, two approaches can be used to advance the $\boldsymbol{E}$ components parallel to the layer when M Debye media are present in the cell. One approach by discretising one $(M+1)$-order differential equation, the other by discretising M 2-order differential equations identical to the auxiliary equation used at the regular nodes of the Debye medium. In the experiments reported in this paper, we used the latter solution relying on a set of M 2-order differential equations. The actual FDTD algorithm corresponding to this solution is provided with details in Section III. In the case of a thin layer in a vacuum, we also performed the calculations with (13a). Section V shows that equation (13a), exact when only one Debye medium is present in the FDTD cell, can provide us with an acceptable approximation of the solution when several Human-Body Debye media are present in the cell.

III. The Thin Layer FDTD Update Equations

A. The Update Equations for the Components Inside the Thin Layer

We formulate the update equations for E_y, E_z and H_x inside the layer. If we consider E_z, M equations for $D_{z_m}^{n+1}$ ($1 \le m \le M$) can be obtained by discretising (15) in time domain as in

$$D_{z_m}^{n+1} = \alpha_{1_m} E_z^{n+1} - \alpha_{2_m} E_z^n + \alpha_{3_m} E_z^{n-1} + \beta_{1_m} D_{z_m}^n - \beta_{2_m} D_{z_m}^{n-1} \quad (16)$$

where

$$\alpha_{1_m} = \frac{2\epsilon_0\epsilon_{\infty_m}\tau_m + 2(\epsilon_0\epsilon_{\mathrm{S}_m} + \sigma_m\tau_m)\Delta t + \sigma_m(\Delta t)^2}{2(\Delta t + \tau_m)},$$
$$\alpha_{2_m} = \frac{-\sigma_m(\Delta t)^2 + 4\epsilon_0\epsilon_{\infty_m}\tau_m + 2(\epsilon_0\epsilon_{\mathrm{S}_m} + \sigma_m\tau_m)\Delta t}{2(\Delta t + \tau_m)},$$
$$\alpha_{3_m} = \frac{\epsilon_0\epsilon_{\infty_m}\tau_m}{\Delta t + \tau_m},$$
$$\beta_{1_m} = \frac{\Delta t + 2\tau_m}{\Delta t + \tau_m}, \qquad \beta_{2_m} = \frac{\tau_m}{\Delta t + \tau_m}.$$

Utilising (7) and (16), Ψ_z^{n+1} can be rewritten as

$$\Psi_z^{n+1} = \sum_{m=1}^{M} s_m(\alpha_{1_m} E_z^{n+1} - \alpha_{2_m} E_z^n + \alpha_{3_m} E_z^{n-1} + \beta_{1_m} D_{z_m}^n - \beta_{2_m} D_{z_m}^{n-1}). \quad (17)$$

When $M = 3$, by making E_z^{n+1} the subject of (17), we obtain

$$E_z^{n+1} = \gamma_1(\Psi_z^{n+1} + \gamma_2 E_z^n - \gamma_3 E_z^{n-1} - \gamma_4 D_{z_1}^n + \gamma_5 D_{z_1}^{n-1} - \gamma_6 D_{z_2}^n + \gamma_7 D_{z_2}^{n-1} - \gamma_8 D_{z_3}^n + \gamma_9 D_{z_3}^{n-1}) \quad (18)$$

where

$$\gamma_1 = (\alpha_{1_1} s_1 + \alpha_{1_2} s_2 + \alpha_{1_3} s_3)^{-1},\ \gamma_4 = s_1\beta_{1_1},\ \gamma_7 = s_2\beta_{2_2},$$
$$\gamma_2 = (\alpha_{2_1} s_1 + \alpha_{2_2} s_2 + \alpha_{2_3} s_3), \quad \gamma_5 = s_1\beta_{2_1},\ \gamma_8 = s_3\beta_{1_3},$$
$$\gamma_3 = (\alpha_{3_1} s_1 + \alpha_{3_2} s_2 + \alpha_{3_3} s_3), \quad \gamma_6 = s_2\beta_{1_2},\ \gamma_9 = s_3\beta_{2_3}.$$

After the calculation of E_z^{n+1} in (18), we can use E_z^{n+1} to compute $D_{z_1}^{n+1}$, $D_{z_2}^{n+1}$ and $D_{z_3}^{n+1}$ in (16).

E_y^{n+1} is obtained from (18) and $D_{y_m}^{n+1}$ ($m = 1 \sim 3$) from (16) with z replaced with y.

The update equation for H_x is obtained via the Maxwell-Faraday equation of

$$\oint_C \boldsymbol{E} dl = -\iint_S \mu \frac{\partial \boldsymbol{H}}{\partial t} ds, \quad (19)$$

which yields, at node $H_{x(i,j-\frac{1}{2},k)}$ in Fig. 2. Therefore,

$$E_{y(i,j-\frac{1}{2},k-\frac{1}{2})}\Delta y + E_{z(i,j,k)}\Delta z - E_{y(i,j-\frac{1}{2},k+\frac{1}{2})}\Delta y - E_{z(i,j-1,k)}\Delta z = -\frac{\partial H_{x(i,j-\frac{1}{2},k)}}{\partial t}\iint_S \mu ds. \quad (20)$$

With $\iint_S \mu ds = \mu\Delta y\Delta z$ in mind, (20) can be manipulated as

$$\frac{E_{y(i,j-\frac{1}{2},k-\frac{1}{2})} - E_{y(i,j-\frac{1}{2},k+\frac{1}{2})}}{\Delta z} + \frac{E_{z(i,j,k)} - E_{z(i,j-1,k)}}{\Delta y} = -\mu\frac{\partial H_{x(i,j-\frac{1}{2},k)}}{\partial t} \quad (21)$$

which is the regular FDTD update equation.

In the case when the thin layer is perpendicular to y or z direction, the update equations are (16), (18) and (21) with circular permutations of coordinates.

The advance of the fields inside the layer can be summarised as follows:

1) Compute $\boldsymbol{H}^{n+\frac{1}{2}}$ using the normal FDTD equation
2) Compute quantity $\boldsymbol{\Psi}^{n+1}$ using (8),
3) Compute $\boldsymbol{E}^{n+1}$ using (18) and then $\boldsymbol{D}^{n+1}$ using (16).

The updates (16) and (18) can be applied as well as a special case with a thin Debye layer surrounded with a vacuum where $\epsilon_{\mathrm{S}} = \epsilon_\infty = 1$ and $\sigma = 0$. In this case, (16) yields the trivial solution $D_{z_m}^{n+1} = \epsilon_0 E_z^{n+1}$.

B. The Update Equations for the Components Adjacent to the Thin Layer

For E_x, H_y and H_z which are located half-cell away from the thin layer, the FDTD equations are left unchanged. Consider, for example, the calculation of the $H_{y(i-\frac{1}{2},j,k)}$ as illustrated in Fig. 3.

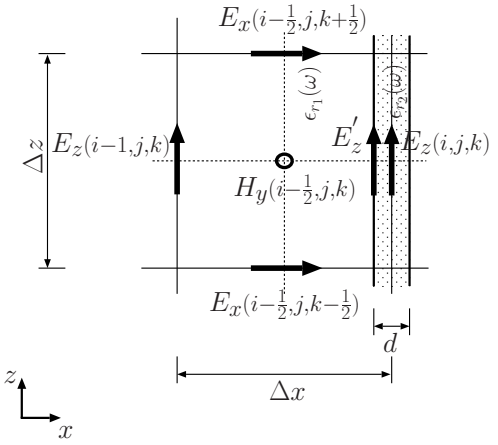

Fig. 3. The field components for calculation of H_y

The standard FDTD equation can not be applied in this area, since H_y and E_x are discontinuous at the physical interface. However, E_z is continuous at the interface. Hence, E_z at the interface, denoted as E'_z, can be calculated by linear interpolation as

$$E'_{z(i,j,k)} = E_{z(i,j,k)} - (E_{z(i,j,k)} - E_{z(i-1,j,k)})\frac{d}{2\Delta x}. \quad (22)$$

Then, applying (19) to the contour yields

$$E_{z(i-1,j,k)}\Delta z + E_{x(i-\frac{1}{2},j,k+\frac{1}{2})}(\Delta x - \frac{d}{2}) - E'_{z(i,j,k)}\Delta z - E_{x(i-\frac{1}{2},j,k-\frac{1}{2})}(\Delta x - \frac{d}{2}) = -\mu\frac{\partial H_{y(i-\frac{1}{2},j,k)}}{\partial t}\Delta z(\Delta x - \frac{d}{2}). \quad (23)$$

Substituting E'_z in (22) into (23) gives the regular FDTD update equation

$$\frac{E_{x(i-\frac{1}{2},j,k+\frac{1}{2})} - E_{x(i-\frac{1}{2},j,k-\frac{1}{2})}}{\Delta z} - \frac{E_{z(i,j,k)} - E_{z(i-1,j,k)}}{\Delta x} = -\mu\frac{\partial H_{y(i-\frac{1}{2},j,k)}}{\partial t}. \quad (24)$$

For the advance of H_z, we can follow the same logic and find the same update equations as in a vacuum. In addition, the advance of E_x involves only H_y and H_z. As they remain outside the layer, applying (5) to E_x gives the regular update equation.

It is worth pointing out that no instability was observed in the numerous 1D and 3D calculations we performed with either one or several Human Body layers in the FDTD cell. This is in accordance with the stability of previous thin layer methods [6]–[12] where instability is not mentioned.

IV. Numerical Experiments

In this section, results computed with the thin layer technique are compared with analytical solutions and reference solutions computed with the FDTD method. The FDTD references were computed using a fine FDTD grid whose space step was equal to the thickness of the layer. In all cases, the thin layer results were computed using the set of (15), *i.e.* with the update equations (16) and (18). The permeability, μ, was set to the vacuum permeability. In the case of one Debye layer in a vacuum, in addition to the solution from (16) and (18) with $\epsilon_{\rm S} = \epsilon_\infty = 1$ and $\sigma = 0$ in two media, we report the solution computed with the discretised form of (13), denoted as "Thin layer using (13)" in the figures. We also report in some figures a result computed with the same coarse grid as the one used with the thin layer calculation, but with a thick layer whose thickness equals the space step. This result is denoted as "Thick layer in coarse grid". It demonstrates the error which would result from the assumption that a thin layer is one cell in thickness when its physical thickness is shorter than the FDTD cell.

A. 1D Numerical Experiments

We considered a plane wave with x-directed propagation and z-directed $\boldsymbol{E}$ field. In this case, only E_z and H_y exist along x direction. The excitation waveform for all experiments was a Gaussian pulse $g(t) = 100[\exp -((t - 5\mathfrak{T})/\mathfrak{T})^2]$ where $\mathfrak{T} = 0.1$ ns and the frequency range of interest is up to 5 GHz. We considered three different simulation scenarios as depicted in Fig. 4. Debye media parameters of the human tissues used in the experiments and their skin depths, δ, and wavelengths, λ, at 5 GHz are provided in Table I.

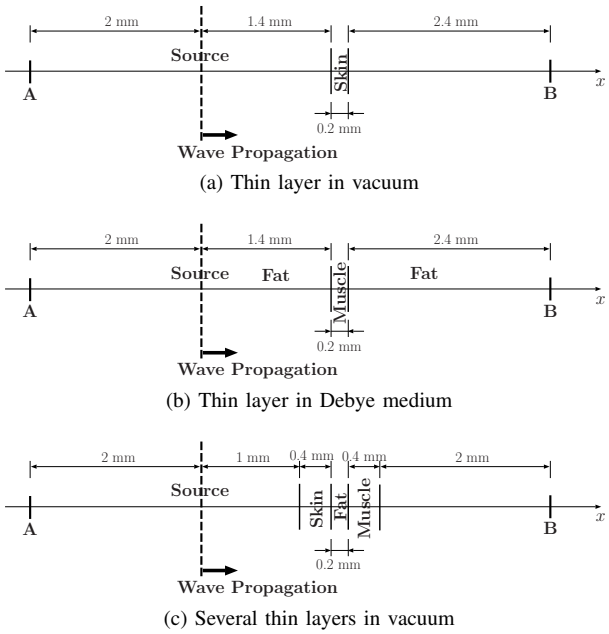

(a) Thin layer in vacuum

(b) Thin layer in Debye medium

(c) Several thin layers in vacuum

Fig. 4. Simulation settings for the one-dimensional experiments.

TABLE I
Media parameters, skin depths and wavelengths

Media	σ (S/m)	$\epsilon_{\rm S}$	ϵ_∞	τ (ps)	At 5 GHz	
					δ (mm)	λ (mm)
Fat	0.037	5.53	4.00	23.6	49.4	26.8
Skin	0.540	47.9	29.9	43.6	10.9	9.88
Muscle	0.747	56.9	28.0	18.7	8.88	8.43

For the thin layer technique, the FDTD steps were $\Delta x = 1$ mm and $\Delta t = 1.7$ ps. For the fine grid reference, we set $\Delta x = 0.2$ mm and $\Delta t = 0.34$ ps. The wave was introduced in the FDTD space using the total-field/scattered-field method. In each simulation, E_z was recorded to observe the reflected wave at A and the transmitted wave at B.

1) Thin layer in vacuum: Fig. 5 shows results for the simple

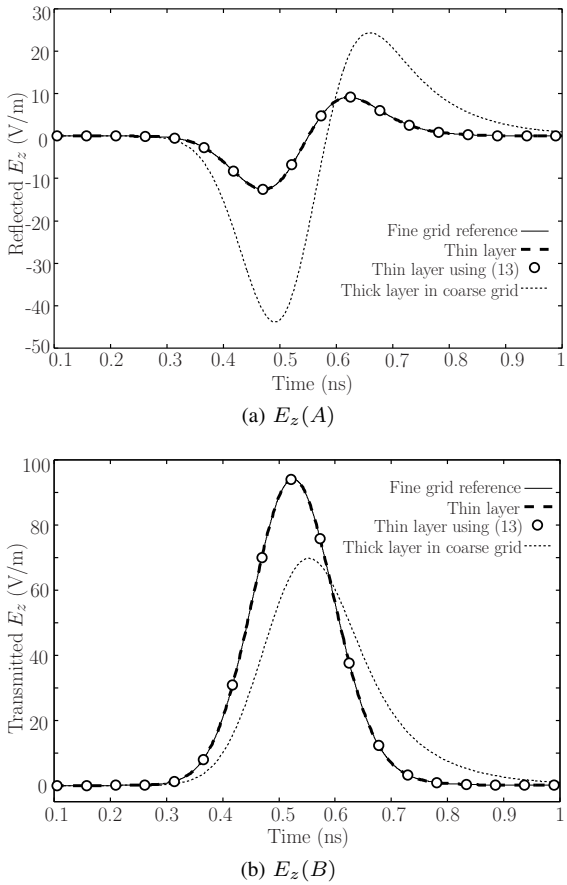

(a) $E_z(A)$

(b) $E_z(B)$

Fig. 5. For the problem in Fig. 4(a) with a thin layer in vacuum, comparison of the thin layer technique relying on (16) and (18), the thin layer technique relying on the discretised form of (13), a fine grid reference solution, and a layer one cell in thickness in the coarse grid, which means a layer 1 mm in thickness in place of its physical thickness of 0.2 mm.

case in Fig. 4(a) where a 0.2-mm-thick Skin layer is placed in vacuum. The thin layer results are plotted for calculations performed with equations (16) and (18), and with the 1-layer equation (13). The two results are superimposed and they agree very well with the reference solution computed with a fine grid. Conversely, the result computed with a layer whose thickness equals the space step of the coarse grid, that is five times its physical thickness, is strongly erroneous.

2) One thin layer in a Debye medium: In this experiment the thin Debye layer was embedded within another Debye medium that fills the whole computational domain. In the cell where the thin layer is situated, there are three Debye media. Two are identical. The reported results in Fig. 6 were obtained

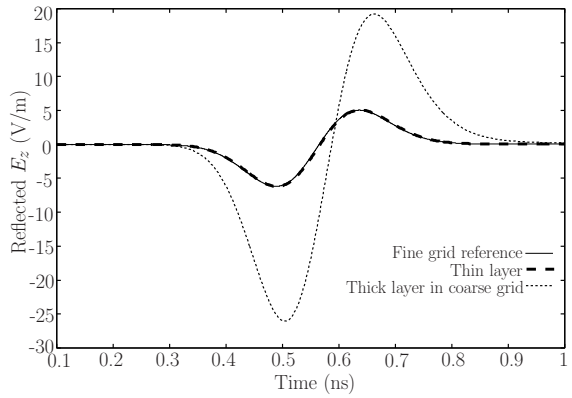

(a) $E_z(A)$

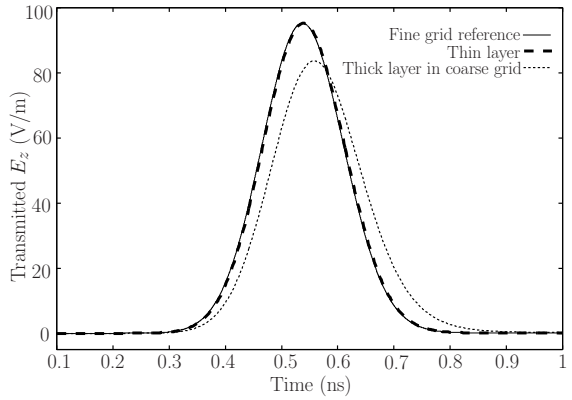

(b) $E_z(B)$

Fig. 6. For the problem in Fig. 4(b) with a thin layer in a Debye medium comparison of the fine grid reference solution with the thin layer technique relying on (16) and (18).

using the general solution (16) and (18). Equation (13) was not used as it is invalid with three Debye media. As with the layer in a vacuum, with the layer in a Debye medium background an excellent agreement is observed with the fine grid reference solution, for both the reflected and the transmitted fields.

3) Several thin layers in vacuum: We considered the presence of three layers in vacuum, 0.4-mm-thick Skin, 0.2-mm-thick Fat and 0.4-mm-thick Muscle layers, as shown in Fig. 4(c). The total thickness equals the FDTD space step of 1 mm. Therefore, there are three Debye layers in the cell and the equations (16) and (18) can be used. The reflected and transmitted fields plotted in Fig. 7 agree very well with the fine grid reference. Notice that if the total thickness of the three layers were thinner than the FDTD cell, four layers would be present in the cell, which would require use of a set of 4 equations, *i.e.* (15) with $M = 4$.

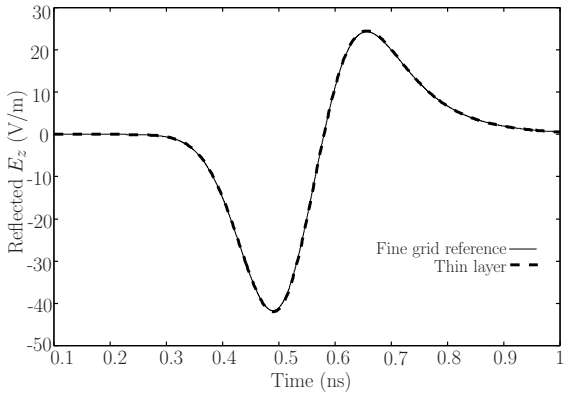

(a) $E_z(A)$

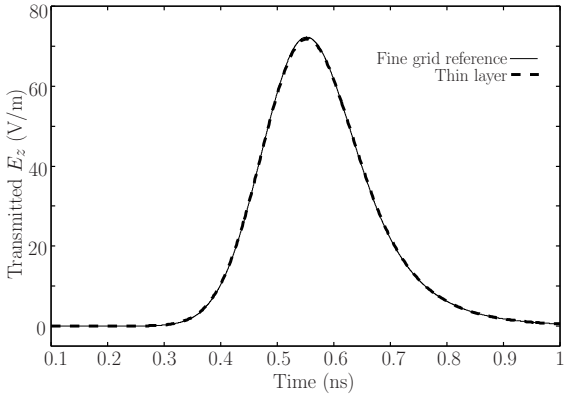

(b) $E_z(B)$

Fig. 7. For the problem in Fig. 4(c) with three thin layers in the FDTD cell, comparison of the fine grid reference solution with the thin layer technique relying on (16) and (18).

B. 1D Numerical vs. Analytical Results

We calculated the reflection and transmission coefficients from the FDTD simulations and compared with analytical solutions for the case where one Debye medium was inserted in vacuum as depicted in Fig. 4(a). The division of the spectrum of each reflected and transmitted waves by the spectrum of the incident Gaussian pulse, $\mathcal{F}\{g(t)\}$, gives the reflection coefficient $|R(f)|$ and the transmission coefficient $|T(f)|$ as a function of frequency. The analytical reflection and transmission coefficients are given by

$$R(f) = r - \frac{r(1-r^2)v^2}{1-r^2v^2}, \tag{25}$$

$$T(f) = \frac{(1-r^2)v}{1-r^2v^2} \tag{26}$$

where

$$r = \frac{(1-n)}{(1+n)}, \qquad v = e^{-j\frac{2\pi}{c}f\,d\,n}, \qquad n = \sqrt{\epsilon_r(f)}$$

where c is the speed of light, d is the layer thickness and $\epsilon_r(f)$ is (1). Fig. 8 shows $|R(f)|$ and $|T(f)|$ from the FDTD

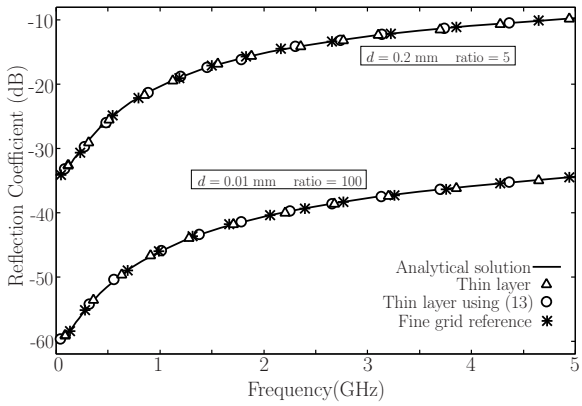

(a) $|R(f)|$

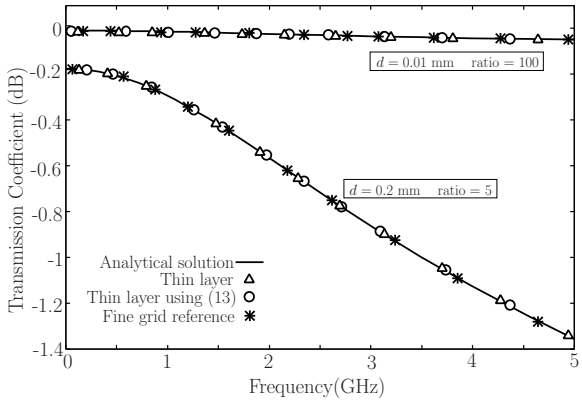

(b) $|T(f)|$

Fig. 8. The analytical solutions compared with the thin layer calculations for two layer-thickness/cell-size ratios.

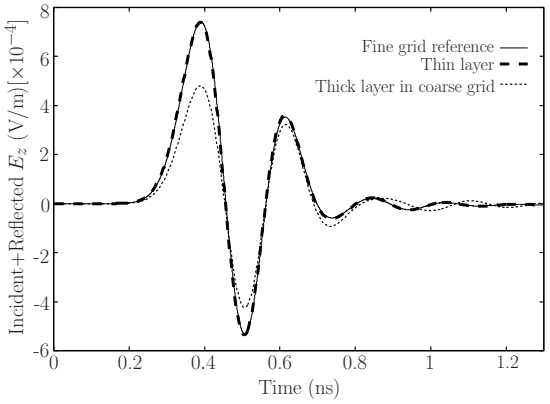

(a) $E_z(A)$

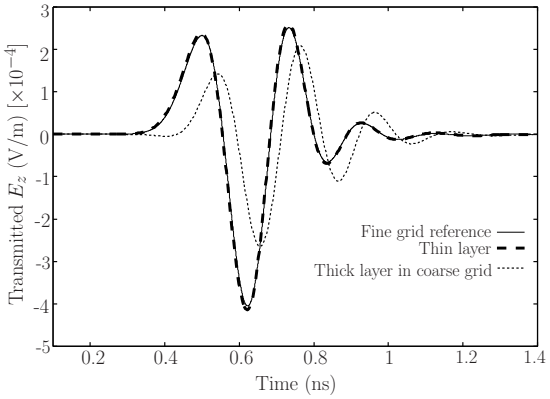

(b) $E_z(B)$

Fig. 10. Observations at A and B in Fig. 9.

simulation and the analytical solution for Skin layers of thicknesses 0.2 mm and 0.01 mm.

The computed results and the analytical solutions agree very well for both layer thicknesses. In most experiments in the paper, the ratio of the cell size to the layer thickness is only 5, because this is a realistic ratio in view of Human Body applications. However, the accuracy of the method is preserved when the ratio is larger, as demonstrated with the experiment reported in Fig. 8 with ratio 100.

C. 3D Numerical Experiment

A 18-mm × 13-mm × 10-mm Bone surrounded by 0.4-mm-thick Fat and 0.2-mm-thick Skin layers was placed in vacuum as depicted in Fig. 9. The Debye media parameters, skin depths and wavelengths at 5 GHz (σ, ϵ_S, ϵ_∞, τ, δ, λ) of Bone are (0.104 S/m, 14.2, 7.36, 34.1 ps, 16.7 mm, 18.2 mm).

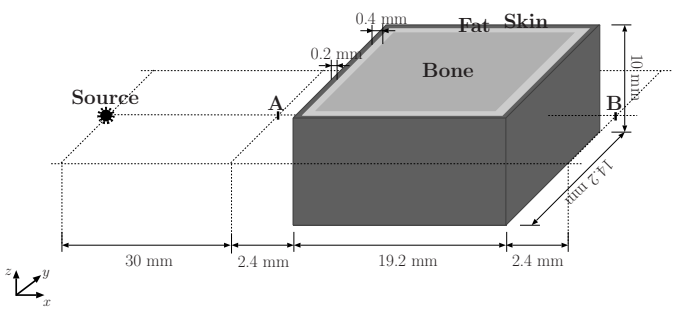

Fig. 9. Simulation settings for the three-dimensional experiment.

Reference solution was obtained by setting $\Delta x = \Delta y = \Delta z = 0.2$ mm and $\Delta t = 0.34$ ps. In the thin layer technique, the sampling was $\Delta x = \Delta y = \Delta z = 1$ mm and $\Delta t = 1.7$ ps. The size of the FDTD space was $380 \times 380 \times 380$ cells with the fine grid calculation whereas it was $92 \times 92 \times 92$ cells with the thin layer technique. The FDTD space was excited using the Gaussian pulse defined in Section IV-A as a point soft source. The object and the observation points, A and B, were on a line parallel to x axis.

Fig. 10 shows the observations for the scenario depicted in Fig. 9. The thin layer technique results are superimposed on the fine grid reference. On the contrary, the result computed with the layers whose thicknesses equal the space step of the coarse grid is substantially different.

V. An Approximate Thin Layer Technique for Human Body Media

In the case of one Debye medium in the FDTD cell, (13) is equivalent to a set of (15). For more than one Debye medium, (11) in time domain becomes a higher order differential equation, *e.g.* a 4-order differential equation for three Debye media. However, if we assume that the relaxation time τ is

the same for all the media, then (11) yields (13) with $\langle \epsilon_\infty \rangle$ and $\langle \epsilon_S \rangle$ equal to weighted averages of ϵ_∞ and ϵ_S in the three media. Therefore, we tried (13) with several human tissues in the FDTD cell, using the same simulation settings shown in Fig. 4(c), and with a unique relaxation time τ set equal to the minimum, maximum or weighted average of τ among those tissues. This approximate method is compared in Fig. 11(a)

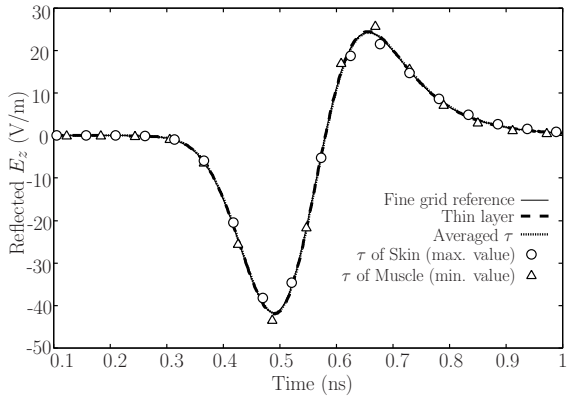

(a) Skin, Fat and Muscle in the cell

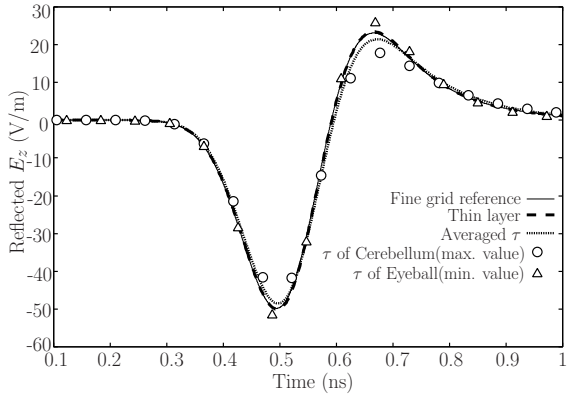

(b) Eyeball, Optical Nerve and Cerebellum in the cell

Fig. 11. Comparison of the approximated solution with the averaged τ, the minimum value of τ, the maximum value of τ, the thin layer technique relying on (16) and (18), and the fine grid reference solution. The incident wave is a 0.1-ns wide Gaussian pulse.

and Fig. 11(b) with the fine grid reference and the solution obtained using (15), *i. e.* (16) and (18). Fig. 11(a) shows the case with a Fat layer between Skin and Muscle in the cell with values of common τ equal to the Skin τ, the Muscle τ, and the averaged τ. The approximate solution with averaged τ gives a good agreement with the fine grid reference in that case. The same test was conducted with different tissues, Eye Ball, Optical Nerve and Cerebellum, whose Debye media parameters, skin depths and wavelengths at 5 GHz, (σ, ϵ_S, ϵ_∞, τ, δ, λ), correspond to (1.44 S/m, 67.7, 10.3, 8.27 ps, 8.06 mm, 7.41 mm), (0.359 S/m, 34.7, 21.0, 36.5 ps — 12.3 mm, 11.4 mm) and (0.826 S/m, 58.2, 35.2, 68.3 ps, 10.3 mm, 9.47 mm), respectively. As seen from Fig. 11(b), the approximate solution with the averaged τ slightly deviates from the fine grid reference. However, for the calculations which do not require the high accuracy, the approximate solution (12)-(13), especially with the averaged τ, could be used.

VI. Conclusion

A subcell modelling technique has been presented for the inclusion of frequency dependent thin layers in the FDTD grid. The layers can be embedded in a frequency dependent background and can be arbitrarily thin. Numerical experiments have demonstrated that the proposed method yields results in close agreement with analytical and reference solutions.

The thin layer method has the potential of providing dramatic reductions of the computational requirements in comparison with calculations with the FDTD cell size equal to the thickness of the layers. More importantly, it will permit to account for more details in calculations with the Human-Body. As an example, at some places of the body the Skin is only 0.1 mm in thickness. With a 0.1-mm FDTD cell, modelling the entire body would require a FDTD domain of the order of 10^{12} cells. Using the subcell technique will allow the FDTD domain to be reduced to a reasonable size, while preserving the exact thickness of the Skin.

References

[1] A. Taflove and S. Hagness, *Computational Electrodynamics: The Finite–Difference Time–Domain Method, third ed.* Boston, MA: Artech House, 2005.

[2] R. Holland and L. Simpson, "Finite-difference analysis of EMP coupling to thin struts and wires," *IEEE Trans. Electromagn. Compat.*, vol. 23, no. 2, pp. 88–97, May 1981.

[3] K. Umashankar, A. Taflove, and B. Beker, "Calculation and experimental validation of induced currents on coupled wires in an arbitrary shaped cavity," *IEEE Trans. Antennas Propag.*, vol. 35, no. 11, pp. 1248–1257, Nov 1987.

[4] J. Gilbert and R. Holland, "Implementation of the thin-slot formalism in the finite-difference EMP code THREDII," *IEEE Trans. Nucl. Sci.*, vol. 28, no. 6, pp. 4269–4274, Dec 1981.

[5] A. Taflove, K. Umashankar, B. Beker, F. Harfoush, and K. Yee, "Detailed FDTD analysis of electromagnetic fields penetrating narrow slots and lapped joints in thick conducting screens," *IEEE Trans. Antennas Propag.*, vol. 36, no. 2, pp. 247–257, Feb 1988.

[6] C. Railton and J. McGeehan, "An analysis of microstrip with rectangular and trapezoidal conductor cross sections," *IEEE Trans. Microw. Theory Tech.*, vol. 38, no. 8, pp. 1017–1022, Aug 1990.

[7] J. Maloney and G. Smith, "The efficient modeling of thin material sheets in the finite-difference time-domain (FDTD) method," *IEEE Trans. Antennas Propag.*, vol. 40, no. 3, pp. 323–330, Mar 1992.

[8] R. Luebbers and K. Kunz, "FDTD modeling of thin impedance sheets," *IEEE Trans. Antennas Propag.*, vol. 40, no. 3, pp. 349–351, Mar 1992.

[9] J. Maloney and G. Smith, "A comparison of methods for modeling electrically thin dielectric and conducting sheets in the finite-difference time-domain (FDTD) method," *IEEE Trans. Antennas Propag.*, vol. 41, no. 5, pp. 690–694, May 1993.

[10] J.-P. Bérenger, "Plaques minces aux différences finies," in *6éme Colloq. Int. Expos. Compat. Electromagn. (CEM) (in French)*, 1992, pp. 298–303.

[11] M. Karkkainen, "Subcell FDTD modeling of electrically thin dispersive layers," *IEEE Trans. Microw. Theory Tech.*, vol. 51, no. 6, pp. 1774–1780, June 2003.

[12] Y.-h. D. B. Wei, S.-Q. Zhang and F. Wang, "A general FDTD algorithm handling thin dispersive layer," *Progress In Electromagnetics Research B*, vol. 18, pp. 243–257, 2009.

[13] V. Nayyeri, M. Soleimani, and O. Ramahi, "A method to model thin conductive layers in the finite-difference time-domain method," *IEEE Trans. Electromagn. Compat.*, vol. 56, no. 2, pp. 385–392, April 2014.

[14] T. Hemmi, F. Costen, S. Garcia, R. Himeno, H. Yokota, and M. Mustafa, "Efficient parallel LOD-FDTD method for debye-dispersive media," *IEEE Trans. Antennas Propag.*, vol. 62, no. 3, pp. 1330–1338, March 2014.

Kenan Tekbas received the M.Sc. degree in Communication Engineering from the University of Manchester, Manchester, U.K., in 2012, and is currently working towards the Ph.D. degree in electrical and electronic engineering in the University of Manchester, Manchester, U.K. His research interests include the finite-difference time-domain method, subcell modelling techniques, computational electromagnetics, bioelectromagnetism and high-performance computing.

Fumie Costen (M'07) received the B.Sc. degree, the M.Sc. degree in electrical engineering and the Ph.D. degree in Informatics, all from Kyoto University, Japan. From 1993 to 1997 she was with Advanced Telecommunication Research International, Kyoto, where she was engaged in research on direction-of-arrival estimation based on Multiple SIgnal Classification algorithm for 3-D laser microvision. She filed three patents from the research in 1999 in Japan. She was invited to give 5 talks in Sweden and Japan during 1996-2014. From 1998 to 2000, she was with Manchester Computing in the University of Manchester, U.K., where she was engaged in research on metacomputing and has been a Lecturer since 2000. Her research interests include computational electromagnetics in such topics as a variety of the finite difference time domain methods for microwave frequency range and high spatial resolution and FDTD subgridding and boundary conditions. She filed a patent from the research on the boundary conditions in 2012 in the U.S.A. Her work extends to the hardware acceleration of the computation using general-purpose computing on graphics processing units, Streaming Single Instruction Multiple Data Extension and Advanced Vector eXtentions instructions. Dr. Costen received an ATR Excellence in Research Award in 1996 and a best paper award from 8th International Conference on High Performance Computing and Networking Europe in 2000.

Jean-Pierre Bérenger (F'09) received a Master in Physics from the University Joseph Fourier, Grenoble, France, in 1973, and a Master in Optical Engineering from the Institut d'Optique Graduate School, Paris, France, in 1975. From 1975 to 2013 he was with the Direction Générale de l'Armement of France, where he was a research engineer on the electromagnetic effects of nuclear rays (1975-1989), he held a position as expert on the electromagnetic effects of nuclear events (1989-1998), and he was a contract manager while staying active in the field of numerical electromagnetic (1998-2013). He is currently a consultant on electromagnetic effects of nuclear rays and on numerical electromagnetics, and a visiting professor at the School of Electrical and Electronic Engineering, the University of Manchester, UK. His researches include low frequency propagation, absorbing boundary conditions, and FDTD method. He is a member of the Electromagnetics Academy and has been an Associate Editor of the IEEE Transactions on Antennas and Propagation from 2006 to 2010. He received the 2013 Medal of URSI-France and the 2014 John Howard Dillinger Gold Medal from URSI.

Ryutaro Himeno received his Doctor of Engineering degree from the University of Tokyo in 1988. In 1979, he joined Central Research Laboratories, Nissan Motor Co., Ltd., Yokosuka, Japan, where he has been engaged in the research of applying Computational Fluid Dynamics analysis to the car aerodynamic development. In 1998, he joined RIKEN and is the director of Advanced Center for Computing and Communication and had been the deputy program director of the Next Generation Computational Science Research Program at RIKEN till April, 2013. He is also a visiting professor at Hokkaido University, Kobe University and Tokyo Denki University. He currently studies Computational Bioengineering, High Performance Computing and blood flows of human bodies. He was a winner of Nikkei Science, Computer Visualization Contest in 2000 and Scientific Visualization Contest in 1996, and received JSME Computational Mechanics Division Award in 1997 and JSME Youth Engineer Award in 1988. He has also received the Paper Award by NICOGRAPH in 1993, Giga FLOPS Award by CRAY Research Inc. in 1990 and other awards.

Hideo Yokota received his Doctor of Engineering degree from the University of Tokyo in 1999. In 1993, he joined Higuchi Ultimate Mechatronics Project, Kanagawa Academy of Science and Technology, Kawasaki, Japan. In 1999, he joined RIKEN and is the contract researcher of Computational biomechanics unit. 2004-2012 Bio-research Infrastructure Construction Team Leader, VCAD system research program, RIKEN. 2007-2012 Cell-scale Research and Development Team Leader,Research Program for Computational Science, RIKEN. 2013-present Image Processing Research Team Leader, Center for Advanced Photonics,RIKEN. He is also a visiting Professor at Hokkaido University, Kobe University, Tokai University and the Tokyo University of Agriculture and Technology. He currently studies biomedical imaging and image processing to the biomedical simulation. Bioimaging Society, Best Image Award, 2005. The Commendation for Science and Technology by the Minister of Education, Culture, Sports, Science and Technology , Young Scientists Prize in 2008.